ELECTRONIC SUPPLEMENTARY MATERIAL

Surface Enhanced Raman Scattering Based on Au Nanoparticles/ Layered Double Hydroxide Ultrathin Films

Rui Tian, Mingwan Li, Haiyan Teng, Heng Luo, Dongpeng Yan,* and Min Wei*

State Key Laboratory of Chemical Resource Engineering, Beijing University of Chemical Technology, Beijing 100029, P. R. China

* Corresponding authors. Fax: +86-10-64425385; Tel: +86-10-64412131.

E-mail: yandongpeng001@163.com (D. Yan); weimin@mail.buct.edu.cn (M. Wei)

LIST OF CONTENTS

1. Morphology of Au NPs

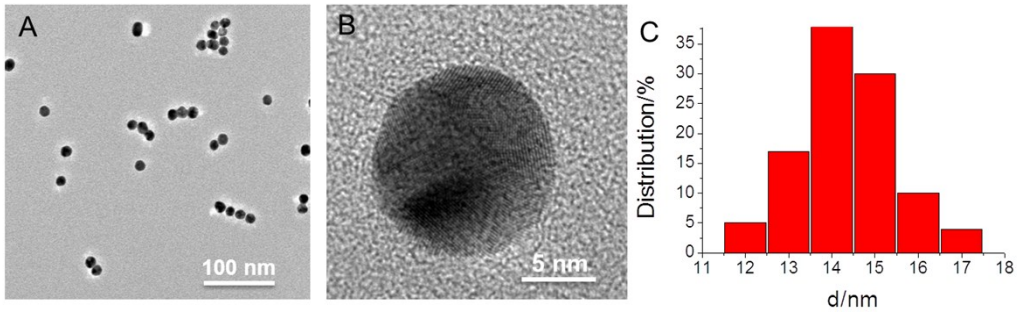

Fig. S1 High resolution TEM images of Au NPs: (A) low magnification and (B) high magnification (with crystal lattice); (C) size distribution of Au NPs.

2. UV-vis absorption spectra of Au NPs colloidal suspension

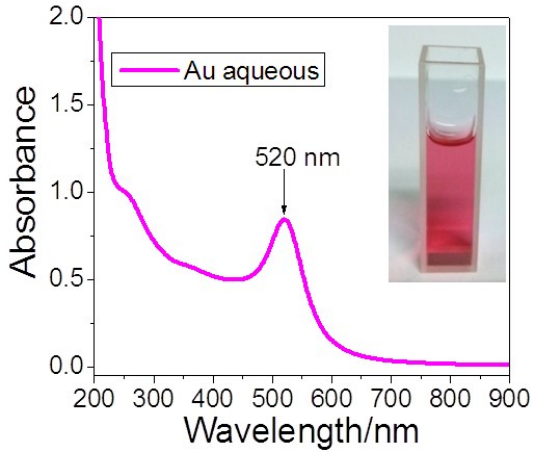

Fig. S2 UV-vis absorption spectrum of Au NPs colloidal suspension (the inset shows its photographs under daylight).

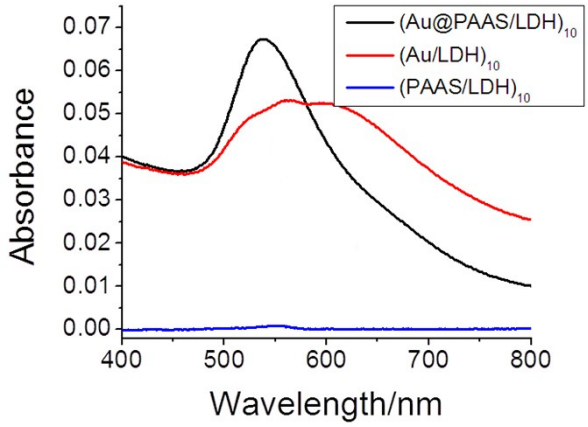

Fig. S3 Comparison of the UV-vis absorption spectra for $(Au@PAAS/LDH)_{10}$ UTF, $(Au/LDH)_{10}$ UTF and $(PAAS/LDH)_{10}$ UTF.

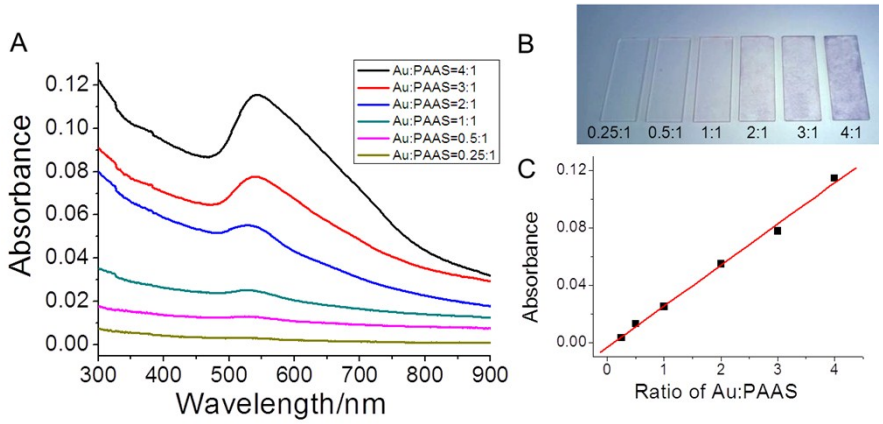

Fig. S4 Characterization of $(Au@PAAS)_{10}$ UTFs with different Au/PAA ratio: (A) UV-Vis absorbance of the assembled UTFs, (B) photograph under daylight, (C) the absorbance at 520 nm as a function of ratio.

3. Morphological characterization of $(Au@PAAS/LDHs)_n$ (n=0–10) UTFs

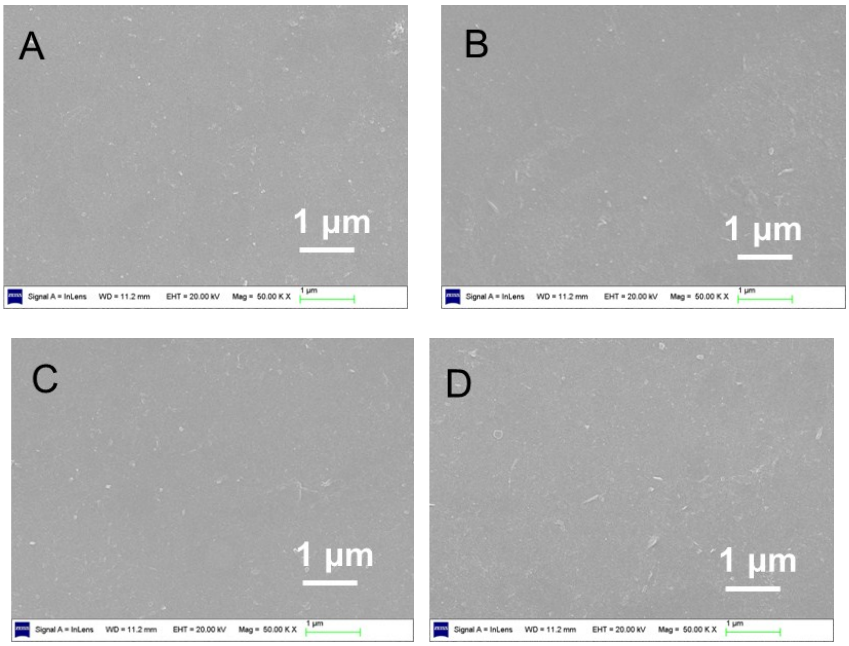

Fig. S5 Top-view SEM images of $(Au@PAAS/LDHs)_n$ (n=0–10) UTFs, from (A) to (D): n=2, 4, 6 and 8, respectively.

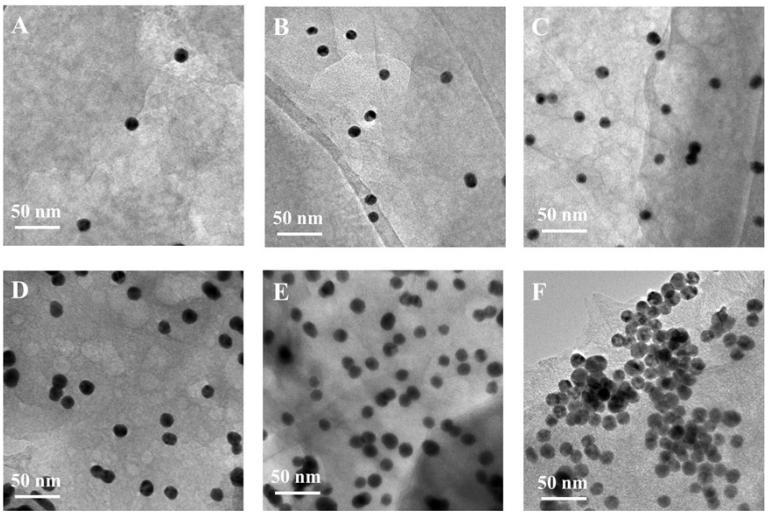

Fig. S6 TEM images of assembled $(Au@PAAS/LDH)_{10}$ UTFs at different Au:PAAS ratio at (A) 0.25, (B) 0.5, (C) 1, (D) 2, (E) 3, (F)4.

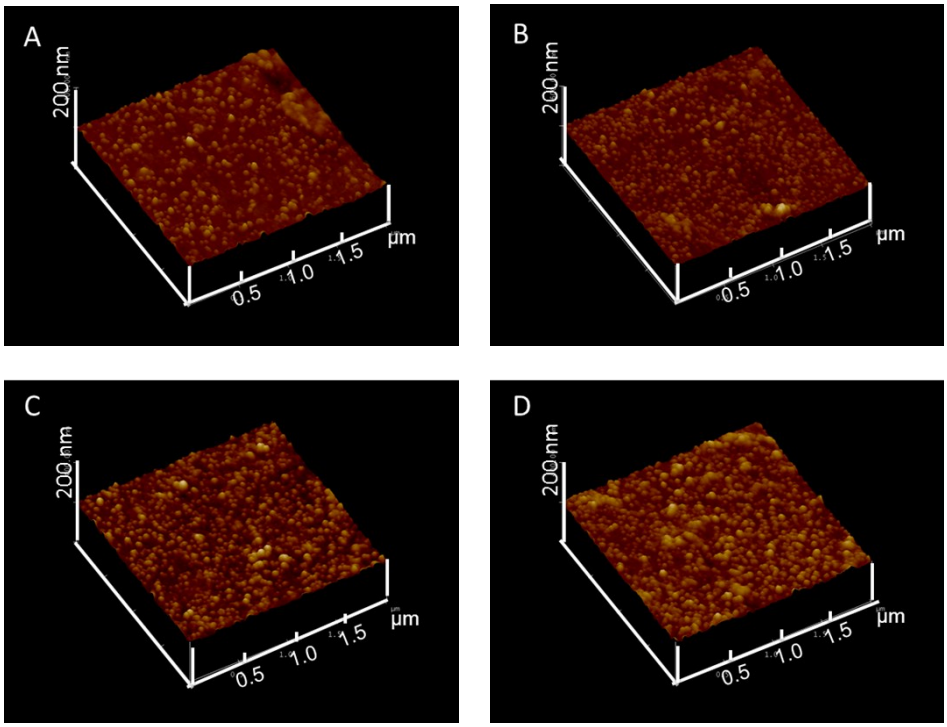

Fig. S7 Tapping-mode AFM topographical images of $(Au@PAAS/LDHs)_n$ (n=0–10) UTFs, from (A) to (D): n=2, 4, 6 and 8, respectively.

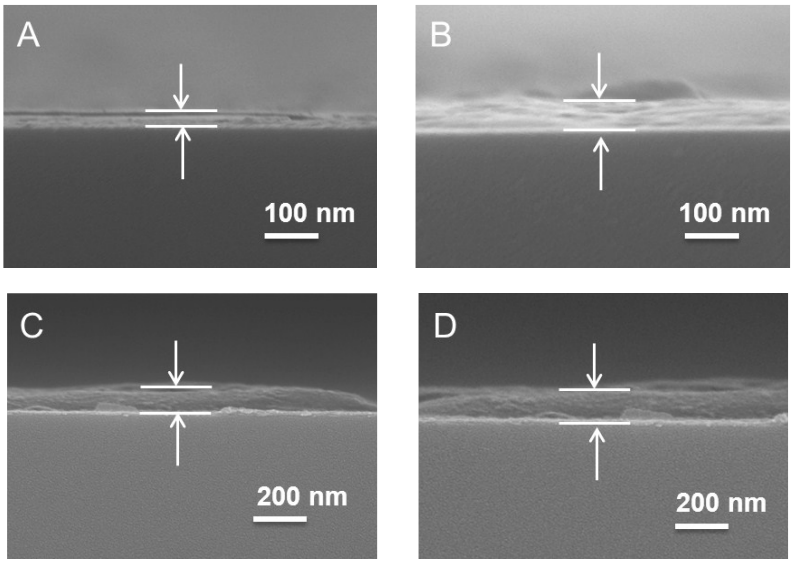

Fig. S8 Side-view SEM images of $(Au@PAAS/LDHs)_n$ (n=0–10) UTFs, from (A) to (D): n=2, 4, 6 and 8, respectively.

Table S1 RMS roughness and thickness parameters for $(Au@PAAS/LDHs)_n$ (n=0–10) UTFs with different bilayer number

n	2	4	6	8	10
RMS roughness/nm[a]	3.60	5.22	7.85	9.02	10.26
SEM thinckness/nm[b]	ca.33	ca.63	ca.98	ca.130	ca.166

[a] The statistical rms roughness values were obtained by AFM, see Fig. S6.

[b] The SEM thickness values were obtained from the side view of $(Au@PAAS/LDHs)_n$ UTFs, see Fig. S7.

4. Role of LDH nanosheets recorded by Raman Spectrum

Table S2 Experimental Raman spectrum of R6G and related assignments

Raman Shift/cm^{-1}	Assignment
609	C–C–C ring in-plane bending
770	C–H out-of-plane bending
1310	aromatic C–C stretching vibration
1360	aromatic C–C stretching vibration
1508	aromatic C–C stretching vibration
1649	aromatic C–C stretching vibration

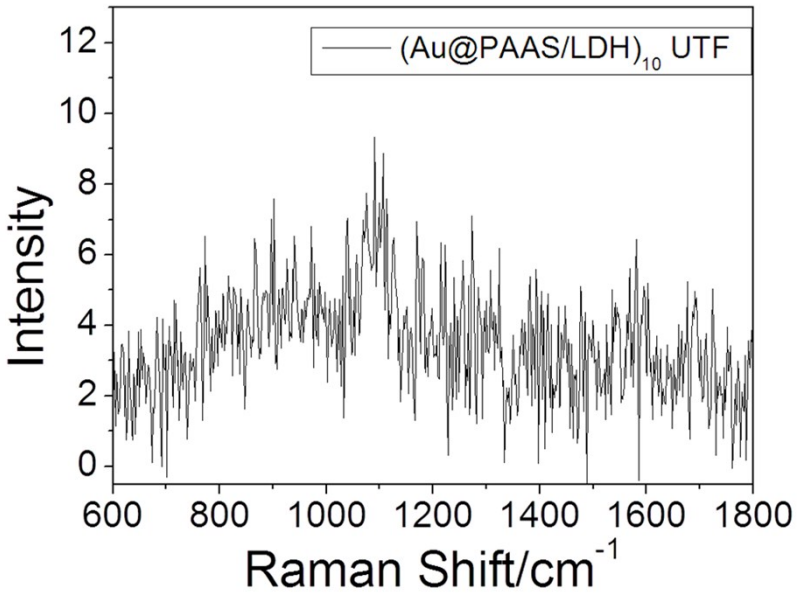

Fig. S9 Raman spectrum of $(Au@PAAS/LDH)_{10}$ UTF as a reference sample.

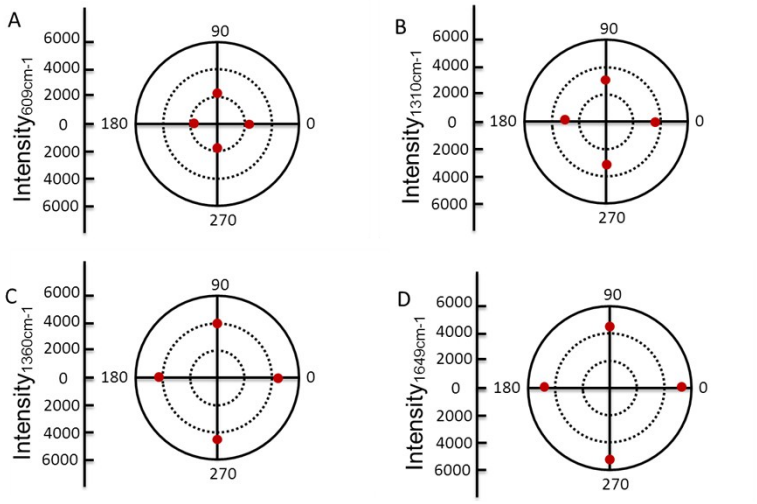

Fig. S10 Polar plots of the SERS intensity at (A) 609 cm^{-1}, (B) 1310 cm^{-1}, (C) 1360 cm^{-1} and (D) 1649 cm^{-1} of R6G as a function of polarization angle.

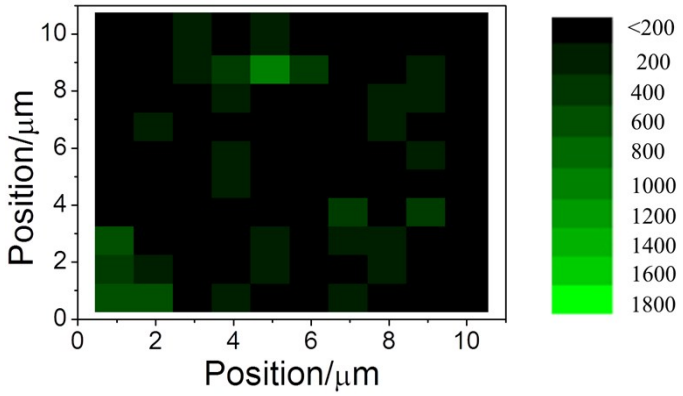

Fig. S11 Raman mapping of $(Au/LDH)_{10}$ loaded R6G.

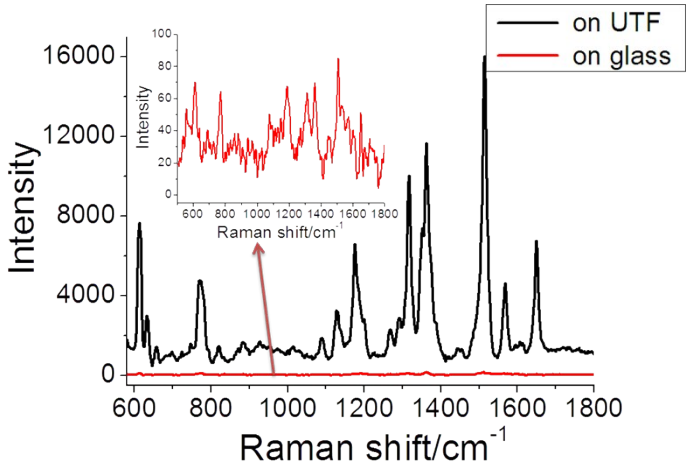

Fig. S12 SERS spectra of 10^{-3} M R6G recorded on glass and $(Au@PAAS/LDH)_{10}$ UTF (the inset shows the enlarged spectrum of R6G on glass).

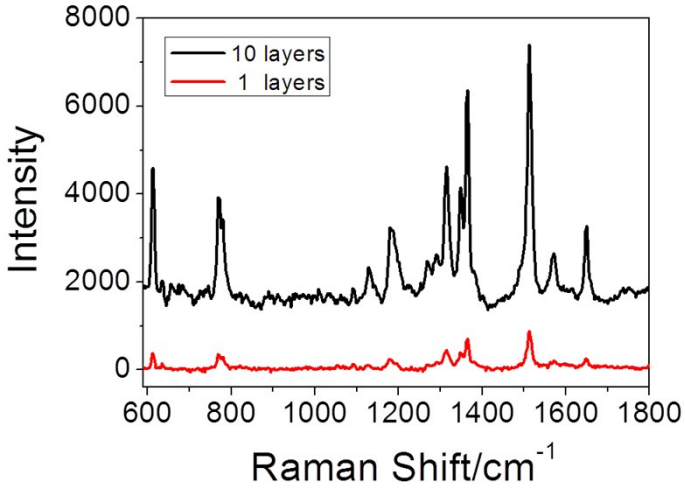

Fig. S13 SERS spectra of $(Au@PAAS/LDH)_n$ at single layer and multilayer.

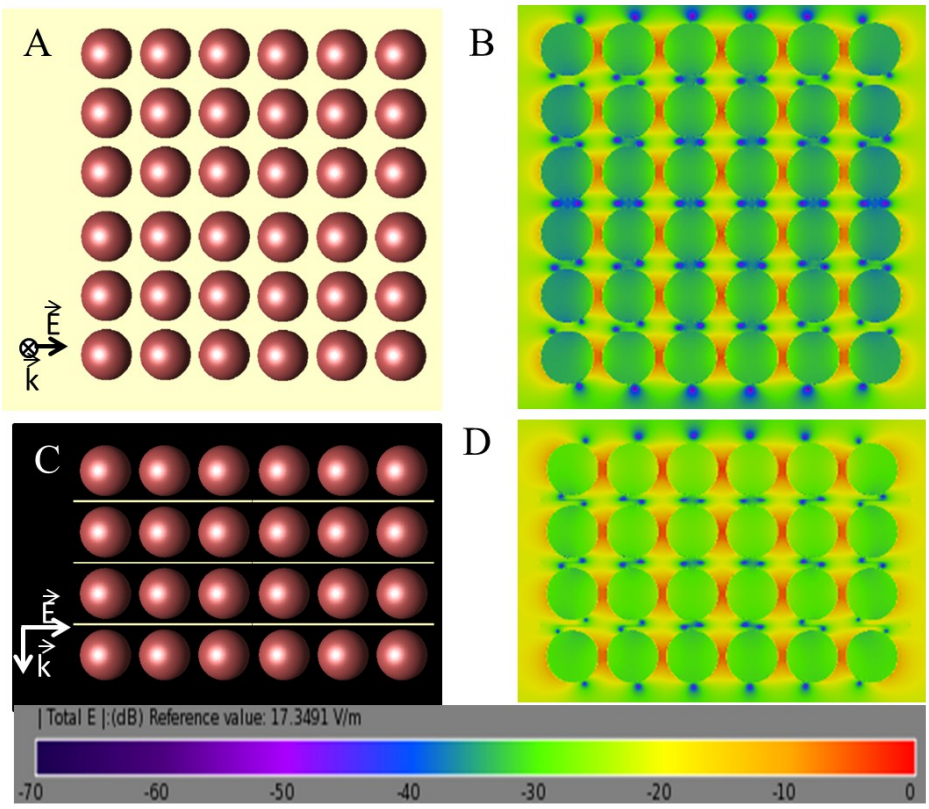

Fig. S14 FDTD model of in (A) *x-y* and (C) *x-z* plane; and calculated spatial distribution of the electric field intensity for (B) *x-y* and (D) *x-z* plane.

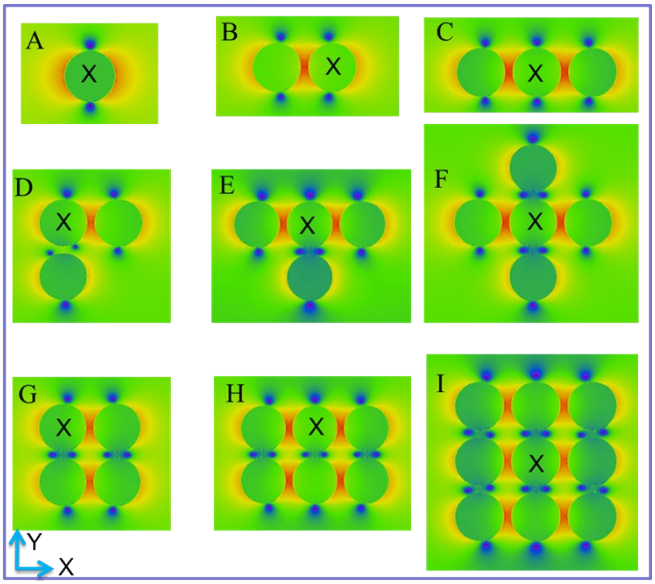

Fig. S15 FDTD simulation for different number of nanopartiples with the light impinged along *z* and polarized in *x* direction for all cases (from A to I, number of particles: 1, 2, 3, 3, 4, 5, 4, 6, 9).

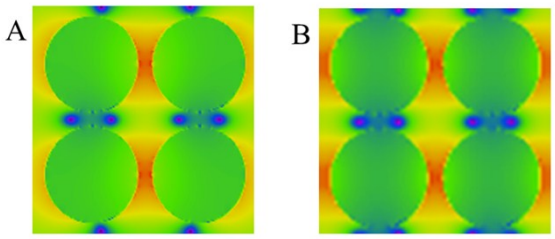

Fig. S16 Local EM field distributions and intensities for (A) a four-particle system of a 2×2 array, (B)a four-particle system in the center of a 6×6 array.

5. Raman spectra of analytes drop-casted on glass substrate

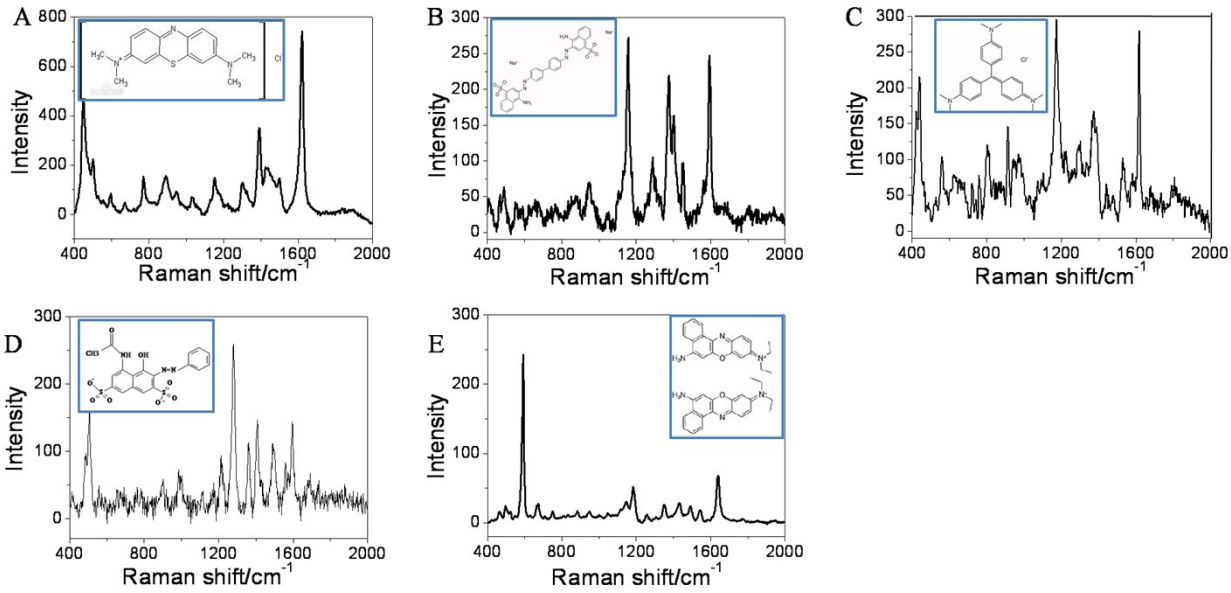

Fig. S17 Raman spectra of different analytes (10^{-2} M) drop-casted on the glass substrate: (A) Methylene blue, (B) Congo red, (C) Crystal violet, (D) Acid red, (E) Nile blue (insets show the molecule structure of the analytes).

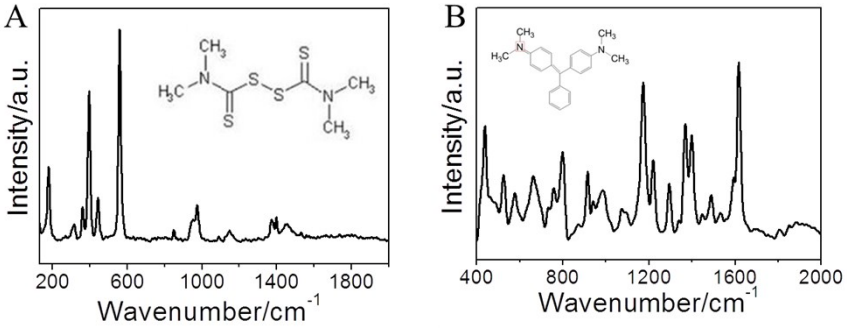

Fig. S18 Raman spectra of chemical residue analytes on the glass substrate: (A) thiram and (B) malachite green (insets show the molecule structure of the analytes).

6. Loading and unloading properties of (Au@PAAS/LDH)$_n$ UTFs

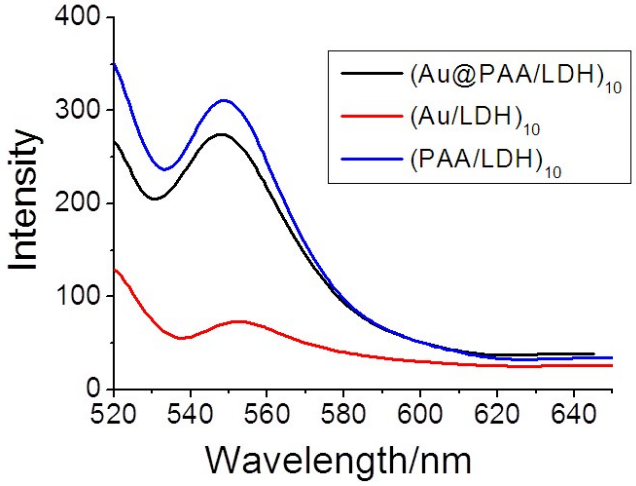

Fig. S19 Fluorescence emission spectra of (Au@PAAS/LDH)$_{10}$, (Au/LDH)$_{10}$ and (PAAS/LDH)$_{10}$ UTF after immersion in R6G solution.

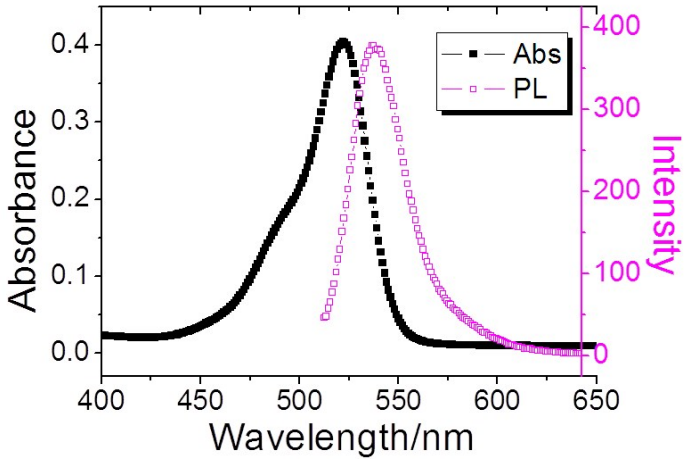

Fig. S20 UV-vis absorption and fluorescence emission spectra of R6G aqueous solution released from the R6G-loaded UTF.

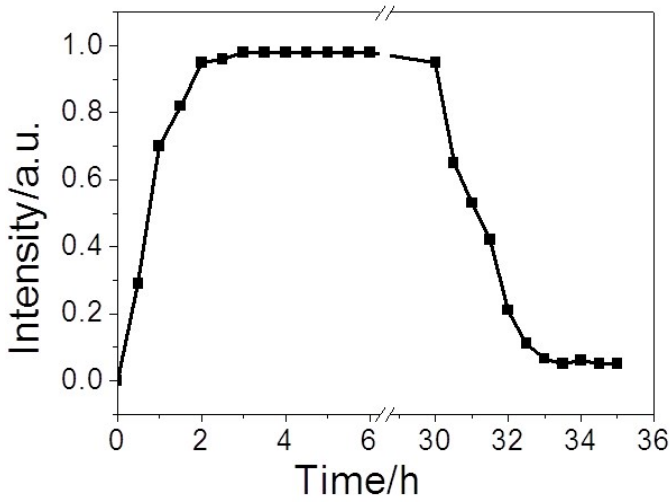

Fig. S21 Fluorescence intensity changes of $(Au@PAAS/LDHs)_{10}$ UTF in the loading and unloading process as a function of time.

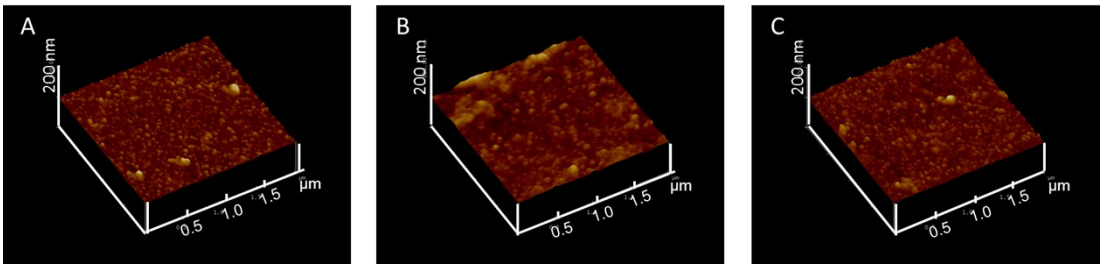

Fig. S22 AFM images of (A) the original $(Au@PAAS/LDH)_{10}$ UTF, (B) the UTF after loading R6G, and (C) the UTF after the release of R6G treated by water.